energies

MDPI

Article

Modeling and Mechanism Investigation of Inertia and Damping Issues for Grid-Tied PV Generation Systems with Droop Control

Yongbin Wu [1], Donghui Zhang [2], Liansong Xiong [3,4,*], Sue Wang [1], Zhao Xu [3] and Yi Zhang [4]

1 School of Electrical and Control Engineering, Shaanxi University of Science & Technology, Xi'an 710021, China; wuyongbin@sust.edu.cn (Y.W.); wangsue@sust.edu.cn (S.W.)
2 School of Electrical and Information Engineering, Hunan University of Technology, Zhuzhou 412008, China; ceozdhceo@163.com
3 Department of Electrical Engineering, Hong Kong Polytechnic University, Hong Kong 999077, China; eezhaoxu@polyu.edu.hk
4 School of Automation, Nanjing Institute of Technology, Nanjing 211167, China; zhangyi6779@163.com
* Correspondence: xiongliansong@163.com; Tel.: +86-136-7911-4072

Received: 23 April 2019; Accepted: 20 May 2019; Published: 23 May 2019

Abstract: Inertia effect and damping capacity, which are the basic characteristics of traditional power systems, are critical to grid frequency stability. However, the inertia and damping characteristics of grid-tied photovoltaic generation systems (GPVGS), which may affect the frequency stability of the grid with high proportional GPVGS, are not yet clear. Therefore, this paper takes the GPVGS based on droop control as the research object. Focusing on the DC voltage control (DVC) timescale dynamics, the mathematical model of the GPVGS is firstly established. Secondly, the electrical torque analysis method is used to analyze the influence law of inertia, damping and synchronization characteristics from the physical mechanism perspective. The research finds that the equivalent inertia, damping and synchronization coefficient of the system are determined by the control parameters, structural parameters and steady-state operating point parameters. Changing the control parameters is the simplest and most flexible way to influence the inertia, damping and synchronization ability of the system. The system inertia is influenced by the DC voltage outer loop proportional coefficient K_p and enhanced with the increase of K_p. The damping characteristic of the system is affected by the droop coefficient D_p and weakened with the increase of D_p. The synchronization effect is only controlled by DC voltage outer loop integral coefficient K_i and enhanced with the increase of K_i. In addition, the system dynamic is also affected by the structural parameters such as line impedance X, DC bus capacitance C, and steady-state operating point parameters such as the AC or DC bus voltage level of the system and steady-state operating power (power angle). Finally, the correctness of the above analysis are verified by the simulation and experimental results.

Keywords: grid-tied photovoltaic generation system; deloading maximum power point tracking; DC voltage control timescale; electrical torque analysis method; inertia and damping characteristics

1. Introduction

In recent years, with the increasingly serious problems of energy crisis and environmental pollution, the need for development of green and clean energy sources has become the consensus of the world [1–3]. Among them, photovoltaic power generation, as one of the most promising power generation technologies, has been widely considered [4].

However, with the increasing penetration of photovoltaic (PV) in the public power grid, large-scale grid-tied PV inverters featuring low inertia and weak damping are being connected to the power

system, which brings severe challenges to the safe and stable operation of the power grid [5,6]. Electric vehicles and distributed energy storage are becoming more and more popular. The source and load boundary of the power grid is more blurred, and there is great uncertainty, which makes the "operation mode" of the power system more diversified, decentralized and differentiated [7]. In the future, renewable energy will need to take responsibility for part of the load balance. At the same time, how to evaluate the inertia, damping and synchronization level of the GPVGS under typical control strategy so as to realize the friendly and compatible connection of renewable energy to the power grid has become an urgent problem to be solved [8].

In view of the inertia and damping mechanism research of renewable energy grid-tied power generation system, reference [9] makes full use of the idea of multi-time scale, grasps the time scale of interest, ignores other dynamic processes, and establishes the mathematical model of the system. Reference [10] divides the dynamic behavior of power electronic grid into three timescale: AC current, DC voltage and mechanical speed. Among them, the inertia characteristic is mainly affected by the DVC timescale dynamic process, so the inertia characteristic of the converter system is mainly to analyze the dynamic process of the DVC timescale.

There are few studies on the inertia, damping and synchronization characteristics of the GPVGS at home and abroad. Reference [11] used virtual synchronous generator (VSG) technology to simulate the characteristics of traditional synchronous machines and improve the standby rotational inertia of the GPVGS. References [12,13] proposed a reactive standby PV-VSG strategy for variable step power tracking to provide inertia and damping support for the PV system. References [11–13] only made the system have certain inertia and damping characteristics from the perspective of the control method, and did not analyze the inertia and damping mechanism affecting the system from the physical mechanism level. In [14], the electric torque analysis method is used to analyze the inertia and damping characteristics of the grid-tied inverter itself, but the influence of the primary side energy was not considered. References [15,16] combined with energy storage devices to analyze the effects of two different control strategies on the inertia and damping characteristics of grid-tied energy storage systems. Based on [11–16], we want to obtain a similar inertia expression (1) for PV systems compared to conventional synchronous generator:

$$J = 2H = 4\pi^3 f \frac{GD^2}{S_N}\left(\frac{n}{60}\right)^2, \quad (1)$$

where J represents the inertia; f is the power frequency; G is the gravitational acceleration; D is the diameter of the object; S_N is the rated system capacity; n is the speed of synchronous generator.

This paper establishes the DVC timescale mathematical model of the GPVGS based on droop control, and uses the electric torque method to reveal the factors and action rules that affect the inertia, damping and synchronization ability of the system from the physical mechanism perspective. It is beneficial to select appropriate control strategies and parameters, so that the GPVGS presents better inertia, damping and synchronization characteristics, to improve the stability of the power system.

2. Research Ideas and Methods

2.1. Definition of DVC Timescale in the GPVGS

As we know, the response time constant of current control is often designed around 10 ms (which is closely related with the switching frequency), and those of DVC and PLL about ten times larger are selected [17]. Further considering the different response speeds of these control loops, the reference [10] extends VSC electromagnetic dynamics into two types, viz., dynamics in current control timescale (around 10 ms) and dynamics in DVC timescale (around 100 ms), as illustrated in Figure 1. For simplicity, dynamics in these two timescales can be analyzed individually, due to their relatively separated response times. Therefore, for DVC timescale dynamic analysis, AC or DC currents timescale dynamic can be considered to instantaneously track their reference values.

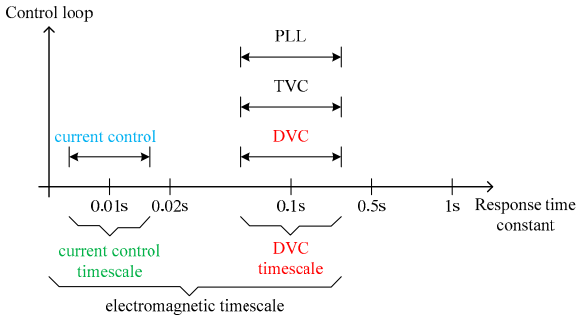

Figure 1. The multi-timescale classification of system.

2.2. Electrical Torque Analysis Method

From the aspects of physical structure, characteristic parameters, physical mechanism and dynamic model of energy transfer process, there is a significant correspondence between the traditional RSG and the new energy grid-tied power generation system. There is a strong similarity among the structure, motion mechanism and mathematical model of system. Therefore, we can learn from classical electric torque analysis method to analyze the influencing factors and action laws affecting the stability of the GPVGS from the physical mechanism perspective [18].

Analogous to the small-signal stability method of the traditional RSG, the DVC timescale dynamic process of the GPVGS can be expressed by the incremental equation [14]:

$$\begin{cases} \frac{\mathrm{d}\Delta\delta}{\mathrm{d}t} = \Delta\omega \\ 2H\frac{\mathrm{d}\Delta U_{\mathrm{dc}}}{\mathrm{dt}} = \Delta P_{\mathrm{in}} - \Delta P_{\mathrm{e}} \end{cases}, \tag{2}$$

where $H = \frac{CU_{\mathrm{dc}}^2}{2S_{\mathrm{B}}}$ is the inertia time constant of the system.

In order to analyze the inertia, damping and synchronization characteristics of the grid-tied inverter system, the static synchronous generator (SSG) model is proposed in literature [14]. The DVC timescale dynamic process of the grid-tied inverter is described by the following standard equation:

$$\begin{cases} \frac{\mathrm{d}\Delta\delta}{\mathrm{d}t} = \Delta\omega \\ T_{\mathrm{J}}\frac{\mathrm{d}\Delta\omega}{\mathrm{dt}} = -T_{\mathrm{D}}\Delta\omega - T_{\mathrm{S}}\Delta\delta \end{cases}, \tag{3}$$

where T_{J}, T_{D}, and T_{S} represent the equivalent inertia, damping, and synchronization coefficient of the SSG, respectively.

The above three parameters are important physical concepts for characterizing the dynamic characteristics of SSG in classical stability theory. The electric torque analysis method based on the above concept can analyze the system stability from the physical mechanism perspective. And T_{J}, T_{D} and T_{S} respectively represent inertia level, damping and synchronization capability of the grid-tied inverter system [14].

3. The Control Strategy of System

3.1. System Description

The main circuit topology and control method of the GPVGS based on droop control is shown in Figure 2. This system consists of a photovoltaic array (PVA), boost converter, and inverter. The boost converter adopts the frequency droop control to simulate the primary frequency modulation process of the prime mover. The inverter adopts the double closed-loop control of the conventional voltage and current to correspond to the rotational synchronous generator (RSG). This control strategy can simulate the traditional peak-regulation power plant when a large proportion of renewable energy is connected to the grid, so that the GPVGS is responsible for the load balancing.

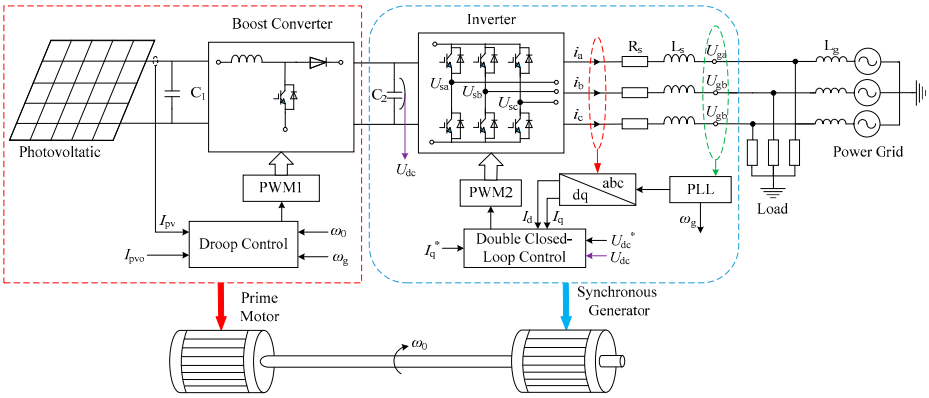

Figure 2. The main circuit topology and control method of the GPVGS based on droop control.

In order to better make the GPVGS respond to the load balancing responsibility, when the power grid fluctuates, the system provides reasonable inertia and damping support, so that the system can reach the power balance as soon as possible. When the maximum output power of the PV is much larger than the system's load power or scheduling demand of power grid, the boost converter adopts the deloading maximum power point tracking (DMPPT) control method and works in the droop control mode to meet the supply and demand balance. When the PV output power is much smaller than the load power or scheduling requirements of power grid, the boost converter can only maintain system stability with the maximum power output.

The characteristic curve of PV-PU is shown in Figure 3. When the power frequency droop control is performed, it can be seen from the PV curve that one power command $P_{1,2}$ at any time corresponds to the output voltages U_1 and U_2 of the two PV panels. However, each terminal voltage has a one-to-one correspondence with power. Therefore, the power frequency droop control can be improved to the frequency droop control. The frequency droop is used to control the PVA output voltage as the outer loop, and the PVA output current is used as the inner loop.

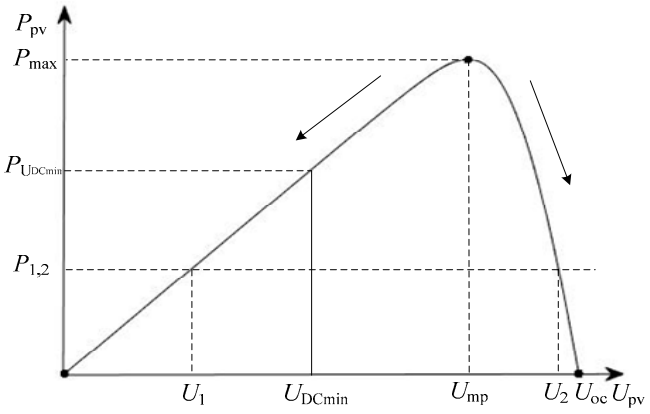

Figure 3. PV P-U characteristic curve.

Taking the maximum power point of the P-U curve as the boundary, the interval (0, U_{mp}) and (U_{mp}, U_{oc}) are opposite to the monotonicity of the power. In the interval (0, U_{mpp}), the output voltage U_{pv} of PVA is positively correlated with the output power P_{pv}, and is limited by the minimum voltage U_{DCmin} of the DC-side inverter failure. Meanwhile, the adjustable power is limited and the adjustment speed is slow. In the interval (U_{mp}, U_{oc}), U_{pv} is negatively correlated with P_{pv}. P_{pv} can be adjusted in a full range. The system sensitivity is good due to the large slope. In order to ensure the safe and stable operation of the GPVGS with operating at a faster adjustment speed in the full power range, (U_{mp}, U_{oc}) is selected as the operating range of the PVA output voltage.

In order to simplify the modeling, according to the U-I curve shown in Figure 4, the output terminal voltage U_{pv} and current I_{pv} of the PVA under the voltage frequency droop control have the problem of repeated control. U_{pv} is multiplied by I_{pv} to determine the output power P_{pv}. To do this, you only need to select one of the variables between U_{pv} and I_{pv} for control. The frequency droop can be used to control I_{pv}, to indirectly control P_{pv}. In order to ensure the stability, speed and full power range of the GPVGS to respond to load balance, this paper takes the interval $(0, I_{mp})$ as an example for related research.

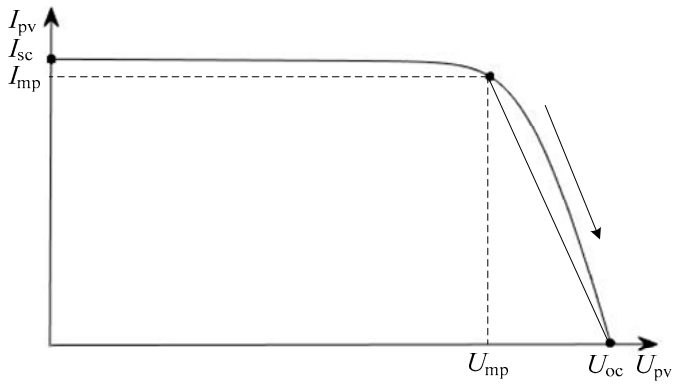

Figure 4. PV U-I characteristic curve.

In this paper, a 10-string and 5-parallel Suntech Power STP200-18-UB-1 is used to form PVA, whose U-I characteristic curve is consistent with Figure 4 at a specific illumination and temperature. The electrical parameters of the PVA under standard conditions are shown in Table 1:

Table 1. Electrical parameters of PVA under standard conditions.

Parameters	Value	Parameters	Value
Open circuit voltage, U_{oc}	334 V	Maximum power point, U_{mp}	262 V
Short circuit current, I_{sc}	40.6 A	Maximum power point, I_{mp}	38.15 A

Reference [19] has proved that the mathematical model of PVA can be linearized. So this approximation method is used in this paper. In the interval $(0, I_{mp})$, the U-I curve shown in Figure 3 can be simplified by a straight line equation. The simplified expression is:

$$I_{pv} = -K_{pv}(U_{pv} - U_{oc}), \tag{4}$$

where K_{pv} is the simplified slope of the U-I curve of $I_{pv} \in (0, I_{mp})$.

The voltage and current output of the PV are linearized as:

$$\Delta U_{pv} = -\frac{1}{K_{pv}}\Delta I_{pv}, \tag{5}$$

3.2. The Control Strategy of Boost Converter

Considering the above factors of the PVA, the control strategy of the PVA and the boost converter is shown in Figure 5. The control strategy is used the frequency droop as the outer ring, and the output current of the PVA as the inner ring. The frequency droop is used to control the output current of the PVA, and indirectly control the output power of the PVA.

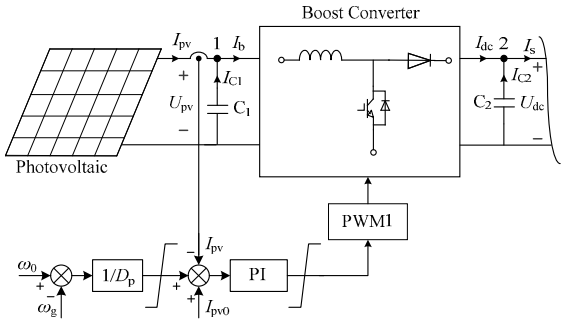

Figure 5. The control diagram of the boost converter.

In the double closed-loop control strategy of frequency and current shown in Figure 5, the bandwidth of the general inner loop is much larger than the outer loop. That is to say, for the frequency control process of the outer loop, the current control timescale dynamic process of the inner loop can be ignored [20]. For the DVC timescale dynamic process, the current output of boost convert can be expressed as:

$$I_{\mathrm{pv}}{}^{*} = I_{\mathrm{pv}} = \frac{1}{D_{\mathrm{p}}}(\omega_0 - \omega_{\mathrm{g}}) + I_{\mathrm{pv0}}, \tag{6}$$

where D_{p} is the droop coefficient, ω_0 is the angular frequency set by the system, ω_{g} is the angular frequency of the real-time detection of the grid, I_{pv0} is the steady-state operating point of the system, and $I_{\mathrm{pv0}} \in (0, I_{\mathrm{mp}})$.

Equation (6) is linearized and can be expressed as:

$$\Delta I_{\mathrm{pv}} = -\frac{1}{D_{\mathrm{p}}}\Delta\omega, \tag{7}$$

For power node 1, capacitance C_1 is similar to LCL filter, and its dynamic response speed is very fast [18]. It belongs to the current control timescale category, and its dynamic process can be ignored, namely:

$$I_{\mathrm{pv}} \approx I_{\mathrm{b}}, \tag{8}$$

For the boost converter, ignoring its own loss, the power both before and after the converter is considered to be constant, i.e.:

$$P_{\mathrm{in}} = U_{\mathrm{pv}}I_{\mathrm{pv}} = U_{\mathrm{dc}}I_{\mathrm{dc}}, \tag{9}$$

For small-signal stability analysis, the incremental relationship among variables is generally considered. Therefore, after linearizing Equation (9), you can get:

$$\Delta P_{\mathrm{in}} = \Delta U_{\mathrm{pv}}I_{\mathrm{pv0}} + U_{\mathrm{pv0}}\Delta I_{\mathrm{pv}} = \Delta U_{\mathrm{dc}}I_{\mathrm{dc0}} + U_{\mathrm{dc0}}\Delta I_{\mathrm{dc}}, \tag{10}$$

where U_{pv0} and I_{pv0} are the steady-state operating point parameters of the PV.

Substituting Equations (5) and (7) into (10), the output power of the boost converter can be linearized as:

$$\Delta P_{\mathrm{in}} = \left(\frac{1}{K_{\mathrm{pv}}}I_{\mathrm{pv0}} - U_{\mathrm{pv0}}\right)\frac{1}{D_{\mathrm{p}}}\Delta\omega, \tag{11}$$

3.3. The Control Strategy of Grid-Connected Inverter

As shown in Figure 6, the grid-tied inverter adopts double closed-loop control strategy of DC voltage outer loop and current inner loop. The DC voltage outer loop is based on the principle of power balance to realize the voltage regulation control of the DC bus. The current loop mainly realizes

the tracking control of the grid side current to realize the sine wave current control of the unit power factor of the grid-connected inverter. At the same time, the grid-tied current is limited to ensure the safe operation of the grid-tied inverter. In the topology of the *L*-type grid-tied inverter, R_s and L_s respectively represent the equivalent series resistance and inductance of the *L*-type passive filter and the grid-tied inverter. And L_g represents the equivalent reactance between the grid-tied inverter and the infinite grid. L_g also represents the strength of the electrical connection between the grid-tied inverter and the infinite grid [21].

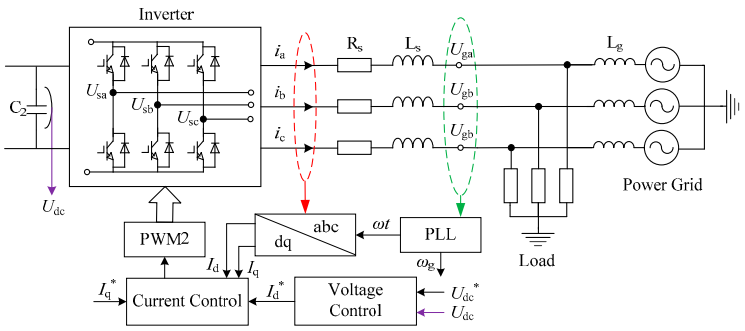

Figure 6. Regular double closed loop control diagram of the grid-connected inverter.

A simplified analysis of the main circuit of the grid-tied inverter is shown in Figure 7. U_s is the excitation potential amplitude of the grid-tied inverter, corresponding to the fundamental component of the outlet voltage before the filter of the grid-tied inverter. δ is the phase angle difference between the grid-tied inverter and the grid terminal voltage. U_g is the amplitude of the grid-tied inverter, which corresponds to the terminal voltage of the grid.

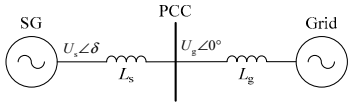

Figure 7. The circuit simplified diagram of the grid-connected inverter.

In the modeling and analysis of grid-tied inverter, a synchronous rotating coordinate system based on grid voltage vector orientation, is often used to make the grid voltage vector U_g coincide with the *d*-axis of the synchronous rotating coordinate system [22], as shown in Figure 8. The excitation potential amplitude U_s of the grid-tied inverter rotates at a synchronous angular frequency ω_0. The grid terminal voltage U_g is rotated according to the angular frequency ω_g with reference to the d-axis. ϕ is the phase difference angle between the terminal voltage and output current of the grid-tied inverter. Φ is the phase angle difference between the excitation potential of the grid-tied inverter and the output current.

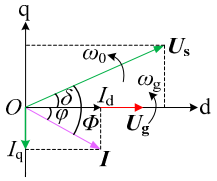

Figure 8. The phasor diagram of grid-connected inverter based on grid voltage orientation.

According to Figure 8, the active power P_e of the grid-tied inverter is:

$$P_e = \frac{3}{2}\frac{U_s U_g}{X}\sin\delta, \tag{12}$$

where: the structural parameter $X \approx \omega_0 L$.

In the grid-tied inverter part, the conventional double closed loop control strategy is adopted. The DVC timescale modeling analysis method can also be adopted. The dynamic process of the current inner loop is ignored, and only the control process of the DC voltage outer loop is considered [23]. In this paper, only the active power part of the GPVGS is analyzed. Therefore, in the control block diagram of Figure 6, the reactive current reference I_q^* is set to 0, and the dynamic process of the active current I_d can be expressed as:

$$I_d^* = I_d = -\left(K_p + \frac{K_i}{s}\right)(U_{dc}^* - U_{dc}), \tag{13}$$

where K_p and K_i are the PI parameters of the DC voltage outer loop.

4. Dynamic Characteristics Analysis of the GPVGS

4.1. SSG Model of the GPVGS

In order to study the inertia, damping and synchronization characteristics of the GPVGS, the above research method are used as the theoretical basis to establish the SSG model of the GPVGS based on droop control.

Firstly, from the phasor diagram illustrated in Figure 8, it is easy to get:

$$I_d = \frac{U_s}{X}\sin\delta, \tag{14}$$

Combining Equations (13) and (14), we can get:

$$\frac{U_s}{X}\sin\delta = -\left(K_p + \frac{K_i}{s}\right)(U_{dc}^* - U_{dc}), \tag{15}$$

For the small-signal stability analysis, linearizing Equation (15) to obtain:

$$sK\Delta\delta = \left(sK_p + K_i\right)\Delta U_{dc}, \tag{16}$$

where $K = \frac{U_s}{X}\cos\delta_0$, which is determined by the structural parameter and the steady-state operating point parameters of the system.

Linearizing Equation (12), it can be expressed as:

$$\Delta P_e = \frac{3}{2}KU_g\Delta\delta, \tag{17}$$

This paper not only analyzes the DVC timescale dynamic process of the grid-tied inverter, but also considers the dynamic effects of the PVA and the boost converter. Substituting Equations (11), (16) and (17) into (2), the SSG model of the GPVGS based on droop control is:

$$\begin{cases} \frac{d\Delta\delta}{dt} = \Delta\omega \\ \left(2KH + \left(U_{pv0} - \frac{1}{K_{pv}}I_{pv0}\right)\frac{K_p}{D_p}\right)\frac{d\Delta\omega}{dt} = -\left(\frac{3}{2}KK_pU_g + \left(U_{pv0} - \frac{1}{K_{pv}}I_{pv0}\right)\frac{K_i}{D_p}\right)\Delta\omega - \frac{3}{2}KK_iU_g\Delta\delta \end{cases}, \tag{18}$$

Comparing Equation (18) with (3), the equivalent inertia coefficient T_J, the equivalent damping coefficient T_D and the equivalent synchronization coefficient T_S of the GPVGS based on droop control are respectively expressed as:

$$\begin{cases} T_J = 2KH + \left(U_{pv0} - \frac{1}{K_{pv}}I_{pv0}\right)\frac{K_p}{D_p} = 2\frac{CU_sU_{dc}^2}{S_BX}\cos\delta_0 + \left(U_{pv0} - \frac{1}{K_{pv}}I_{pv0}\right)\frac{K_p}{D_p} \\ T_D = \frac{3}{2}KK_pU_g + \left(U_{pv0} - \frac{1}{K_{pv}}I_{pv0}\right)\frac{K_i}{D_p} = \frac{3}{2}\frac{U_sU_g}{X}K_p\cos\delta_0 + \left(U_{pv0} - \frac{1}{K_{pv}}I_{pv0}\right)\frac{K_i}{D_p} \\ T_S = \frac{3}{2}KK_iU_g = \frac{3}{2}\frac{U_sU_g}{X}K_i\cos\delta_0 \end{cases}, \tag{19}$$

4.2. The Physical law of the System Dynamic Characteristics

According to Equation (19), the inertia, damping and synchronization characteristics of the GPVGS based on droop control are not only affected by the control parameters of the system, but also influenced by the structural parameters and the steady-state operating point parameters of the system.

4.2.1. Influence of Control Parameters

From the perspective of system control parameters, T_J is affected by the droop coefficient D_p and the proportional coefficient K_p of the DC voltage outer loop PI controller. With the decrease of D_p, the stronger of the coupling between the output power of the boost converter and the system frequency. The greater the output power, the stronger the power support effect on the system, and the inertia effect of the system is enhanced. With the decrease of K_p, the weaker of the inertia effect exhibited by the system.

T_D is related to the PI parameter of the DC voltage outer loop and D_p. The damping characteristic is positively correlated with the PI parameter of the DC voltage outer loop. That is to say, with the increase of PI parameter, the system of stability speed and quasi-degree are obviously accelerated to maintain the DC bus voltage. The damping effect of the system is enhanced. The damping characteristic is negatively correlated with D_p. Namely, with the decrease of D_p, the damping effect of the system is stronger.

T_S is only affected by the integral coefficient K_i of the DC voltage outer loop PI controller. The synchronization characteristic is positively correlated with K_i. With the increase of K_i, the synchronization effect of the system is stronger.

4.2.2. Influence of Structural Parameters

From the perspective of system structural parameters, T_J, T_D and T_S are related to structural parameter X. With the decrease of X, the closer the electrical distance between the system and the infinite grid, the stronger the coupling degree of the large grid, the greater the inertia, damping and synchronization capability of the system. Therefore, the inertia, damping and synchronization characteristics of the system can be improved by reducing the line impedance X or reducing the installation distance from the large power grid.

The DC bus capacitor C is related to T_J. With the increase of C, the more energy is stored or released, the stronger the ability to suppress interference, which means that the system inertia is stronger. Therefore, the system inertia can be improved by increasing C [24].

4.2.3. Influence of Steady-State Operating Point Parameters

From the perspective of the steady-state operating point parameters of the system, T_J is related to U_{dc}. With the increase of U_{dc}, the system's inertia is enhanced. This is because the higher voltage, the more energy storage capacity, and the stronger the ability to suppress external interference. U_g affects the damping and synchronization effects of the system. With the increase of U_g, the damping and synchronization ability of the system is enhanced. The steady-state operating point parameters U_s and δ_0 simultaneously affect the inertia, damping and synchronization characteristics of the system. Increasing U_s can simultaneously improve the inertia, damping and synchronization capability of the system. δ_0 should be reasonably selected according to the stability margin of the system and the capacity utilization of the device. It can be seen that the higher the voltage-level of the grid connection, the better the electrical stability of the system. Therefore, for the PV system under the weak system, the grid voltage level should be improved as much as possible to improve the grid-tied stability of the GPVGS [25].

5. Simulation and Experimental Verification

In order to verify the validity of the above control law and the correctness of the analysis conclusion, the simulation model of the GPVGS based on droop control is built by MATLAB/Simulink, and the experimental platform is built by Simulink Real-Time. The simulation and experiment parameters of the system are shown in Table 2. When the system runs at 1 s, the power grid generates a power angle disturbance. The variation law of the DC bus voltage U_{dc} and the electromagnetic power P_e are analyzed under different control parameters and structural parameters, to indirectly express the strength of the system inertia, damping and synchronization characteristics.

Table 2. The system simulation and experimental parameters.

Parameters	Value	Parameters	Value
PV-link capacitor, C_1	100 uF	The rated phase voltage of Grid, U_g	220 V/50 Hz
Boost converter Inductor, L_b	5 mH	The inductance of the L filter, L_s	3 mH
DC-link capacitor, C	6 mF	Grid side line reactance, L_g	5 mH
Boost switching freq.	20 kHz	Inverter switching freq.	10 kHz
DC voltage, U_{dc}	500 V		

5.1. System Inertia Feature Verification

The system inertia is affected by the control parameters D_p and K_p, and are more obvious with the influence of K_p. Under the condition of keeping D_p unchanged, the influence of K_p on the system inertia characteristics is shown in Figure 9. With the increase of K_p, the oscillation amplitude of U_{dc} under disturbance is reduced, and the oscillation period of U_{dc} is increased. It indicates that the system's anti-disturbance capability is enhanced, namely, the system inertia is enhanced.

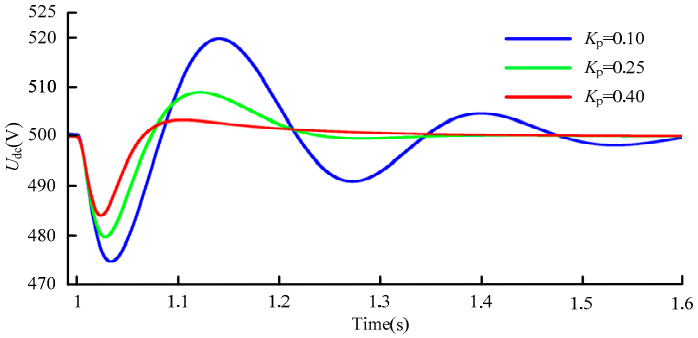

Figure 9. Influence of control parameter K_p on system inertia.

The influence of K_p on P_e is shown in Figure 10. With the increase of K_p, the oscillation amplitude of P_e decreases, the speed of oscillation of P_e recovery balance increases, and the system inertia effect increases. The inertia corresponds to energy, the stronger inertia, the greater the change in P_e. Considering the stability margin limitation of the system, it is not possible to adjust K_p too large to pursue a large inertia, which affects the stable operation of the system.

Experimental results in Figure 11 demonstrate the influence of control parameter K_p on system transient stability. The system retains stability with small variations of K_p value during operation (e.g., K_p increases 0.05 to 0.1), as shown in Figure 11a,b. When K_p increases, the oscillation amplitude of U_{dc} and P_e under disturbance is reduced, and the oscillation period of U_{dc} and P_e is increased. That is to say, the system inertia increases. The simulation results are consistent with the experimental results.

For structural parameters, the system inertia is positively correlated with the DC bus capacitance C. The influence of structural parameter C on the system inertia is shown in Figure 12. With the increase of C, the oscillation amplitude of U_{dc} decreases, the oscillation period of U_{dc} becomes longer, the time for restoring balance becomes longer, and the ability to suppress interference becomes stronger. That is

to say, the system inertia is enhanced. Therefore, the inertia support capability of the system can be improved by increasing the capacitance of the DC bus capacitor *C*.

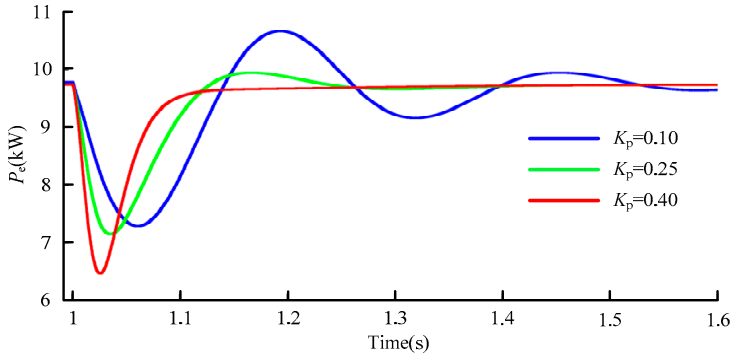

Figure 10. Influence of control parameter K_p on system electromagnetic power P_e.

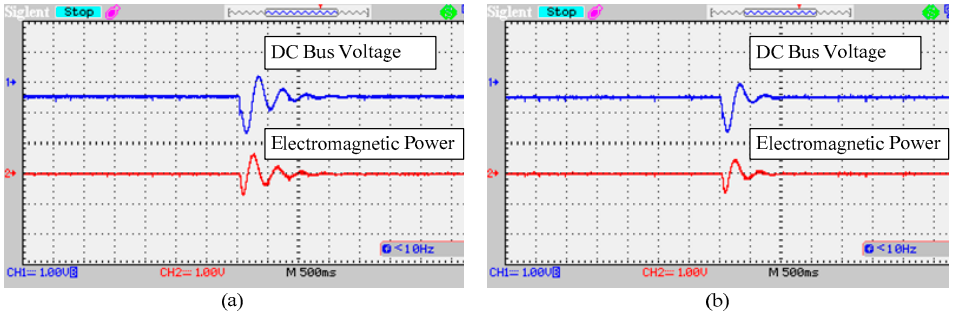

Figure 11. Influence of control parameter K_p on system stability. The K_p increases from (**a**) 0.05 to (**b**) 0.1.

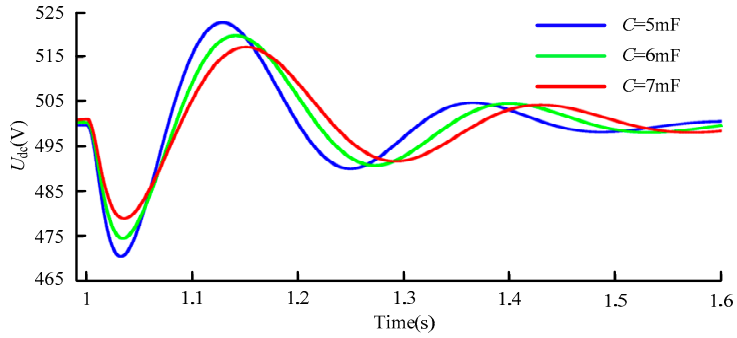

Figure 12. Influence of structure parameter *C* on system inertia.

The influence of *C* on P_e is shown in Figure 13. With the increase of *C*, the oscillation amplitude of P_e decreases, the oscillation speed of P_e decreases, and the speed of the oscillation rises also slows down. Namely, the system inertia is enhanced, and the ability to suppress external disturbances becomes stronger.

Experimental results in Figure 14 demonstrate the influence of structure parameter *C* on system transient stability. The system retains stability with small variations of the DC bus capacitance value during operation (e.g., *C* increases 4 mF to 6 mF), as shown in Figure 14a,b. When *C* increases, the oscillation amplitude of U_{dc} and P_e under disturbance is reduced, and the oscillation period of U_{dc} and P_e is increased. Namely, the system inertia increases. The simulation results are consistent with the experimental results.

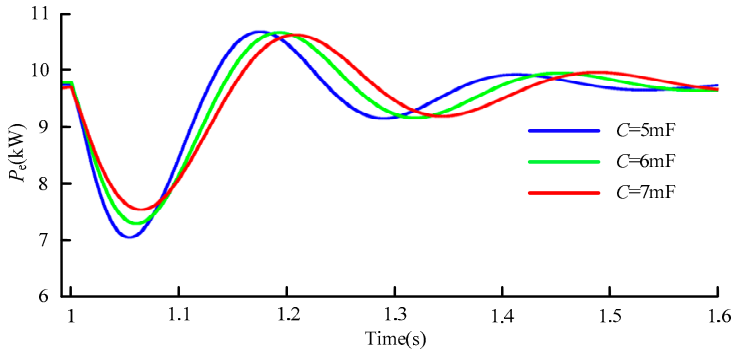

Figure 13. Influence of structure parameter *C* on system electromagnetic power P_e.

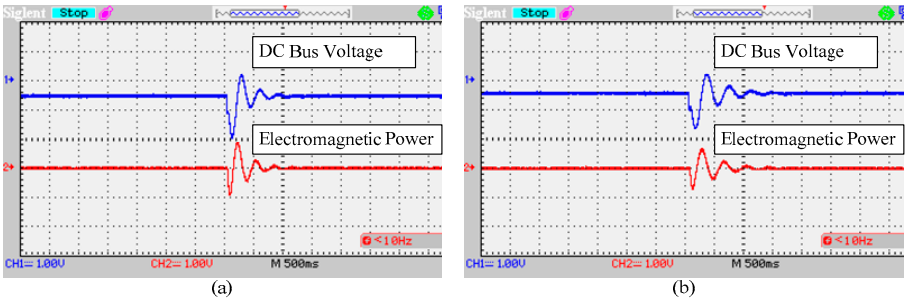

Figure 14. Influence of *C* on system stability. The *C* increases from (**a**) 4 mF to (**b**) 6 mF.

5.2. System Damping Characteristics Verification

The damping characteristics of the GPVGS based on droop control are jointly affected by the control parameters D_p, K_p and K_i, but are more strongly affected by D_p. In the case of keeping K_p and K_i constant, the power angle disturbance is applied to the power grid. The damping characteristic of the system is affected by changing D_p. The simulation result is shown in Figure 15. With the decreases of D_p, the oscillation amplitude attenuation of U_{dc} is significantly enhanced, but the oscillation period of U_{dc} hardly changes. Namely, the damping capacity of the system is stronger.

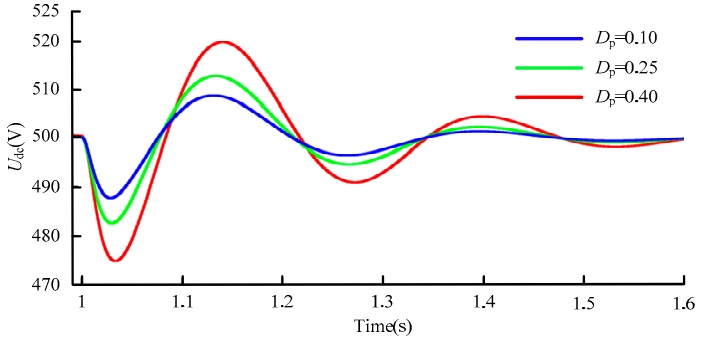

Figure 15. Influence of control parameter D_p on system damping.

The influence of D_p on P_e is shown in Figure 16. With the decreases of D_p, the period of system power oscillation is almost constant, and the attenuation rate of the oscillation amplitude is obviously accelerated. That is to say, the ability to suppress the oscillation is enhanced, and the damping ability is enhanced. From the variation of U_{dc} and P_e, the control parameter D_p has the same effect on the system damping. The stronger the damping capacity, the more obvious the P_e changes.

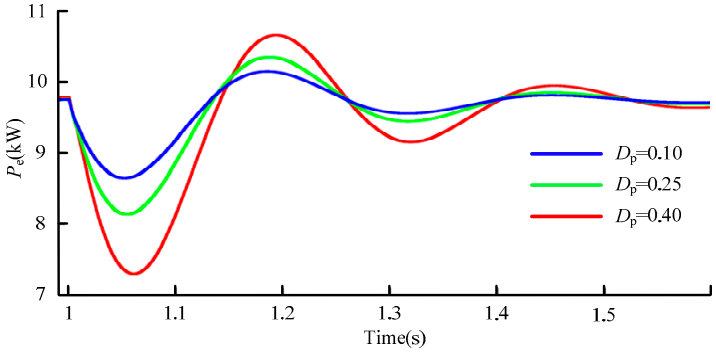

Figure 16. Influence of control parameter D_p on system electromagnetic power P_e.

Experimental results in Figure 17 demonstrate the influence of control parameter D_p on system transient stability. The system retains stability with small variations of D_p value during operation (e.g., D_p increases 4 to 5), as shown in Figure 17a,b. When D_p increases, the oscillation amplitude of U_{dc} and P_e under disturbance is increased, but the oscillation period of U_{dc} and P_e is hardly changed. Namely, the system damping capacity decreases. The simulation results are consistent with the experimental results.

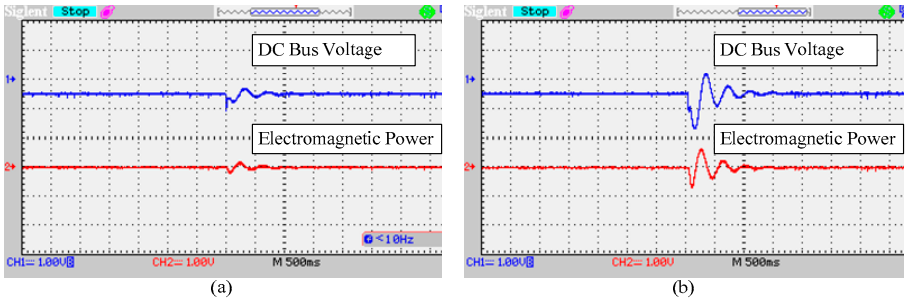

Figure 17. Influence of D_p on system stability. The D_p increases from (**a**) 4 to (**b**) 5.

Under the condition that the control parameters and the steady-state operating point parameters are kept unchanged, the influence law of the structural parameter L on the damping characteristics of the system is shown in Figure 18. With the increase of L, the oscillation amplitude of U_{dc} becomes larger and larger. However, the oscillation period of U_{dc} is obviously unchanged. That is to say, the damping capacity is weaker.

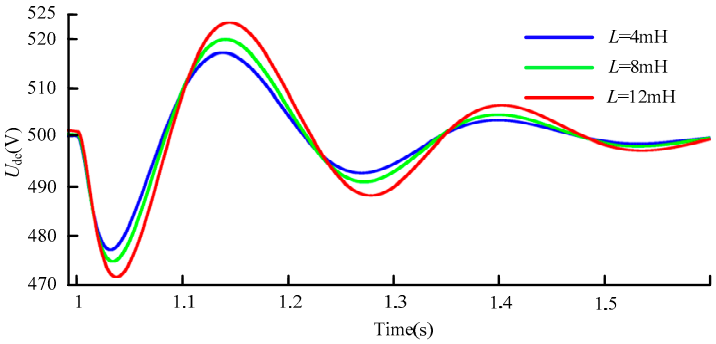

Figure 18. Influence of structure parameter L on system inertia.

The influence of structural parameter L on P_e is shown in Figure 19. With the decreases of L, the oscillation amplitude of P_e becomes smaller and smaller, but the oscillation period of P_e changes insignificantly. It shows that the system damping capacity is stronger. Therefore, the system damping capacity can be improved by reducing inductance L.

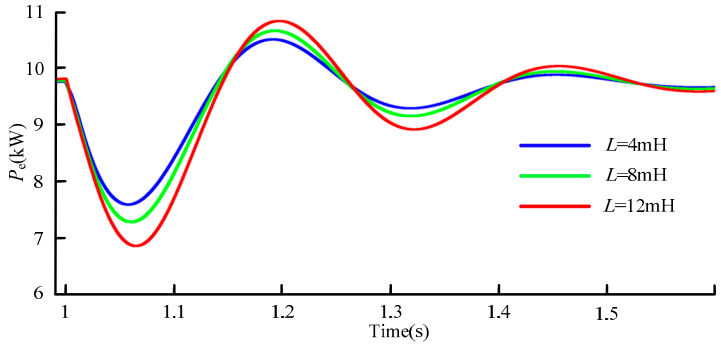

Figure 19. Influence of structure parameter L on system electromagnetic power P_e.

Experimental results in Figure 20 demonstrate the influence of structure parameter L on system transient stability. The system retains stability with small variations of equivalent inductance value during operation (e.g., L increases 4 mH to 8 mH), as shown in Figure 20a,b. When L decreases, the oscillation amplitude of U_{dc} and P_e under disturbance is decreased, but the oscillation period of U_{dc} and P_e is hardly changed. That is to say, the system damping capacity increases. The simulation results are consistent with the experimental results.

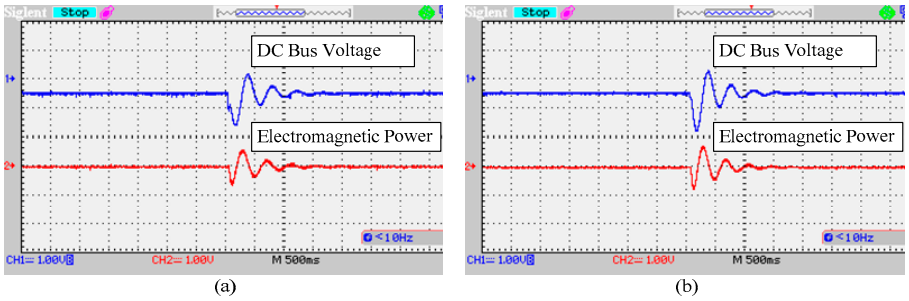

Figure 20. Influence of L on system stability. The L increases from (**a**) 4 mH to (**b**) 8 mH.

5.3. System Synchronization Feature Verification

The synchronization characteristic of the GPVGS based on the droop control is only determined by the control parameter K_i. Figure 21 shows the influence law of changing K_i on the synchronization characteristics of the system under the condition of keeping D_p and K_p unchanged. With the increase of K_i, the oscillation amplitude of U_{dc} is not obvious, but the oscillation period of U_{dc} is obviously shortened, indicating that the synchronization capability of the system is enhanced.

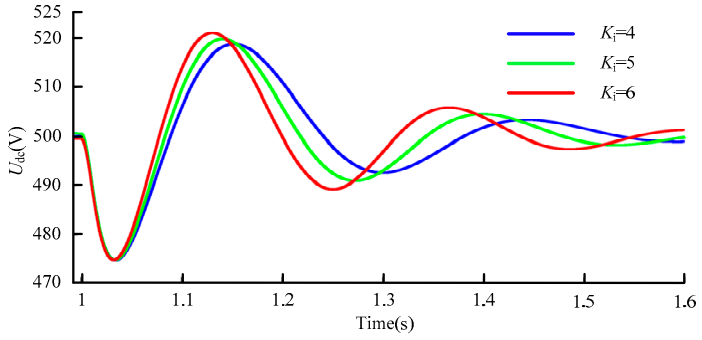

Figure 21. Influence of control parameter K_i on system synchronization.

The influence of K_i on P_e is shown in Figure 22. With the increase of K_i, the oscillation period of P_e changes significantly. While the oscillation amplitude and the attenuation speed of P_e change little,

indicating that the system synchronization effect is enhanced. At the same time, it can be seen that with the enhancement of the system synchronization capability, U_{dc} and P_e change more obviously. The greater the change amplitude of U_{dc}, the greater the change corresponding to P_e. Considering the system dynamic effect speed, K_i should be selected in an appropriate range.

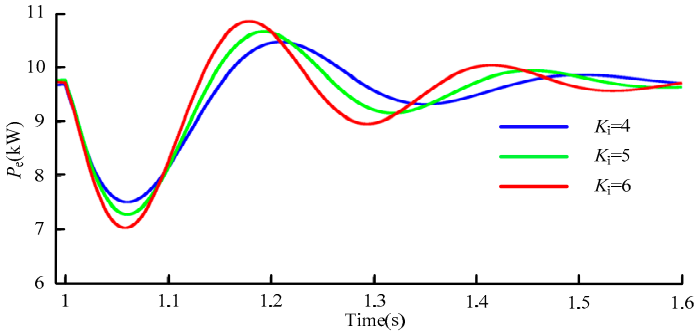

Figure 22. Influence of control parameter K_i on system electromagnetic power P_e.

Experimental results in Figure 23 demonstrate the influence of control parameter K_i on system transient stability. The system retains stability with small variations of K_i value during operation (e.g., K_i increases 4 to 6), as shown in Figure 23a,b. When K_i increases, the oscillation amplitude of U_{dc} and P_e under disturbance is hardly changed, but the oscillation period of U_{dc} and P_e is significant decrease. Namely, the system synchronization capability increases. The simulation results are consistent with the experimental results.

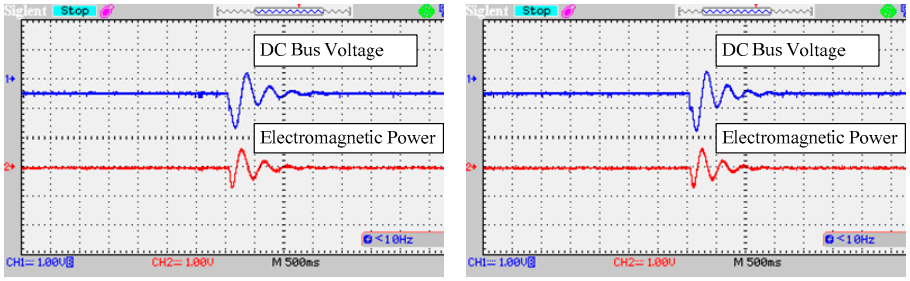

Figure 23. Influence of K_i on system stability. The K_i increases from (**a**) 4 to (**b**) 6.

6. Conclusions and Future Work

In this paper, the GPVGS based on droop control is taken as the research object. The mathematical model of the GPVGS on the DVC timescale dynamics is firstly established. The electric torque method is used to analyze the inertia, damping and synchronization characteristics of the GPVGS from the physical mechanism perspective. The research results show that:

(1) The GPVGS based on droop control also has a certain inertia, damping and synchronization effect. At the same time, the equivalent inertia, damping and synchronization coefficient of the system are affected by the control parameters, structural parameters and steady-state operating points parameters, among which the adjustment control parameters are the simplest way to change the inertia, damping and synchronization characteristics of the system.

(2) From the perspective of control parameters, the inertia characteristics of the system are influenced by the DC voltage outer loop proportional coefficient K_p and positively correlated with K_p. The damping characteristics of the system are affected by the droop coefficient D_p and negatively correlated with D_p. The synchronization effect is only affected by the DC voltage outer loop integral coefficient K_i and positively correlated with K_i.

(3) From the perspective of structural parameters, the system dynamic characteristics are affected by structural parameters such as line impedance X and DC bus capacitance C. Reducing X can improve the inertia, damping and synchronization characteristics of the system. With the increase of C, the system inertia effect is stronger.

(4) From the perspective of steady-state operating point parameters, the system dynamic characteristics are affected by the AC/DC bus voltage level. The higher the voltage level of the bus, the stronger the grid-connected stability of the system.

(5) The GPVGS operating in MPPT mode do not have inertia and damping characteristics. The system can only provide inertia effects when coupled with the grid frequency.

The above research conclusions can be used as the theoretical basis of engineering practice, and the inertia, damping and synchronization characteristics of the GPVGS are rationally designed to make them more friendly to the grid.

Author Contributions: All the authors conceived of and designed the study. Y.W. and D.Z. performed the theoretical analysis and wrote the manuscript with the guidance from L.X., S.W. and Z.X.; Y.W., D.Z. and Y.Z. conceived and designed the simulation experiments.

Funding: This research was supported by the National Natural Science Foundation of China (Grant No. 51577110), the Open Research Fund of Jiangsu Collaborative Innovation Center for a Smart Distribution Network, Nanjing Institute of Technology (Grant No. XTCX201711), Shaanxi Province Industrial Science and Technology Research Project (2015GY038) and Xi'an Science and Technology Plan Project (2017068CG/RC031 (SXKD009)).

Conflicts of Interest: The authors declare no conflict of interest.

References

1. Yang, X.; Song, Y.; Wang, G.; Wang, W. A comprehensive review on the development of sustainable energy strategy and implementation in China. *IEEE Trans. Sustain. Energy* **2010**, *1*, 57–65. [CrossRef]
2. Blaabjerg, F.; Teodorescu, R.; Liserre, M.; Timbus, A. Overview of control and grid synchronization for distributed power generation systems. *IEEE Trans. Ind. Electron.* **2006**, *53*, 1398–1409. [CrossRef]
3. Morjaria, M.; Anichkov, D.; Chadliev, V.; Soni, S. A grid-friendly plant: The role of utility-scale photovoltaic plants in grid stability and reliability. *IEEE Power Energy Mag.* **2014**, *12*, 87–95. [CrossRef]
4. Mei, S.; Zheng, T.; Chen, L.; Li, C.; Si, Y.; Guo, Y. A comprehensive consensus-based distributed control strategy for grid-connected PV-VSG. In Proceedings of the 2016 35th Chinese Control Conference (CCC), Chengdu, China, 27–29 July 2016; pp. 10029–10034.
5. Alipoor, J.; Miura, Y.; Ise, T. Power System Stabilization Using Virtual Synchronous Generator with Alternating Moment of Inertia. *IEEE J. Emerg. Sel. Top. Power Electron.* **2015**, *3*, 451–458. [CrossRef]
6. Vega-Garita, V.; Sofyan, M.F.; Narayan, N.; Ramirez-Elizondo, L.; Bauer, P. Energy management system for the photovoltaic battery integrated module. *Energies* **2018**, *11*, 3371. [CrossRef]
7. Xie, X.; Wang, X.; Hu, J.; Xu, L.; Bongiorno, M.; Miao, Z.; Molinas, M.; Pota, H.; Rodriguez, P. Guest Editorial: Oscillations in power systems with high penetration of renewable power generations. *Iet Renew. Power Gen.* **2019**, *13*, 1–3.
8. Qiu, H.; Fang, J.; Tang, Y. Explore the capability of power electronic converters in providing power system virtual inertia. In Proceedings of the 2018 IEEE Energy Conversion Congress and Exposition (ECCE), Portland, OR, USA, 23–27 September 2018.
9. Hu, J.; Yuan, H.; Yuan, X. Modeling of DFIG-Based WTs for Small-Signal Stability Analysis in DVC Timescale in Power Electronized Power Systems. *IEEE Trans. Energy Convers.* **2017**, *32*, 1151–1165. [CrossRef]
10. Yuan, H.; Yuan, X.; Hu, J. Modeling of Grid-Connected VSCs for Power System Small-Signal Stability Analysis in DC-Link Voltage Control Timescale. *IEEE Trans. Power Syst.* **2017**, *32*, 3981–3991. [CrossRef]
11. Fang, J.; Li, X.; Tang, Y. Grid-connected power converters with distributed virtual power system inertia. In Proceedings of the 2017 IEEE Energy Conversion Congress and Exposition (ECCE), Cincinnati, OH, USA, 1–5 October 2017.
12. Yan, X.; Li, J.; Wang, L.; Zhao, S.; Li, T.; Lv, Z.; Wu, M. Adaptive-MPPT-based control of improved photovoltaic virtual synchronous generators. *Energies* **2018**, *11*, 1834. [CrossRef]

13. Shintai, T.; Miura, Y.; Ise, T. Oscillation damping of a distributed generator using a virtual synchronous generator. *IEEE Trans. Power Del.* **2014**, *29*, 668–676. [CrossRef]
14. Xiong, L.; Zhuo, F.; Wang, F.; Liu, X.; Chen, Y.; Zhu, M.; Yi, H. Static synchronous generator model: A new perspective to investigate dynamic characteristics and stability issues of grid-tied PWM inverter. *IEEE Trans. Power Electron.* **2016**, *31*, 6264–6280. [CrossRef]
15. Ding, G.; Gao, F.; Tian, H.; Ma, C.; Chen, M.; He, G.; Liu, Y. Adaptive DC-link voltage control of two-stage photovoltaic inverter during low voltage ride-through operation. *IEEE Trans. Power Electron.* **2016**, *31*, 4182–4194. [CrossRef]
16. Xiu, L.; Xiong, L.; Yang, P.; Kang, Z. Inertial and damping characteristics of DC distributed power systems based on frequency droop control. *Energies* **2018**, *11*, 2418. [CrossRef]
17. Harnefors, L.; Bongiorno, M.; Lundberg, S. Input-Admittance Calculation and Shaping for Controlled Voltage-Source Converters. *IEEE Trans. Ind. Electron.* **2007**, *54*, 3323–3334. [CrossRef]
18. Xiong, L.; Wang, D. Research on suppression mechanism of STATCOM on power oscillations. In Proceedings of the 2017 IEEE 3rd International Future Energy Electronics Conference and ECCE Asia (IFEEC 2017-ECCE Asia), Kaohsiung, Taiwan, 3–7 June 2017; pp. 806–811.
19. Xiong, L.; Li, Y.; Zhu, Y.; Yang, P.; Xu, Z. Coordinated control schemes of super-capacitor and kinetic energy of DFIG for rystem Frequency Support. *Energies* **2018**, *11*, 103. [CrossRef]
20. Liu, J.; Miura, Y.; Ise, T. Comparison of dynamic characteristics between virtual synchronous generator and droop cntrol in inverter-based distributed generators. *IEEE Trans. Power Electron.* **2016**, *31*, 3600–3611. [CrossRef]
21. Xiong, L.; Xu, Z.; Xiu, L. Energy storage system control for electromechanical oscillation mitigation and its impact on inertia and damping of power system. In Proceedings of the 2018 IEEE 4th Southern Power Electronics Conference (SPEC), Singapore, 10–13 December 2018; pp. 1–5.
22. Fang, J.; Li, H.; Tang, Y.; Blaabjerg, F. On the inertia of future more-electronics power systems. *IEEE J. Emerg. Sel. Top. Power Electron.* **2018**, 1–19. [CrossRef]
23. Guo, K.; Fang, J.; Tang, Y. Autonomous DC-Link Voltage Restoration for Grid-Connected Power Converters Providing Virtual Inertia. In Proceedings of the 2018 IEEE Energy Conversion Congress and Exposition (ECCE), Portland, OR, USA, 23–27 September 2018.
24. Fang, J.; Li, H.; Tang, Y.; Blaabjerg, F. Distributed power system virtual inertia implemented by grid-connected power converters. *IEEE Trans. Power Electron.* **2018**, *33*, 8488–8499. [CrossRef]
25. Gan, D.; Xin, H.; Liu, Y.; Wang, Z.; Yang, T. A new frequency regulation strategy for photovoltaic systems without energy storage. *IEEE Trans. Sustain. Energy* **2013**, *4*, 985–993.